Scientia Iranica, Vol. 8, No. 4, pp 265–276

SCIENTIA
IRANICA

Free-Form 3-D Surface Description in Multiple Scales

F. Mokhtarian*, N. Khalili[1] and P. Yuen[1]

In this paper, a new technique for multi-scale smoothing of a free-form 3-D surface is presented. This technique is a non-trivial generalization of the *Curvature Scale Space* (CSS) representation for 2-D contours. The CSS shape descriptor has been selected to be a part of the MPEG-7 package of standards. Complete triangulated models of 3-D objects are constructed (through fusion of range images) and, then, described at multiple scales. This is achieved by convolving local parameterizations of the surface with 2-D Gaussian filters iteratively. The method, presented here, for local parameterization makes use of semigeodesic or geodesic polar coordinates as a natural and efficient way of sampling the local surface shape. It is demonstrated that smoothing techniques using semigeodesic coordinates and geodesic polar coordinates produce similar results. The smoothing eliminates surface noise and details gradually. During the smoothing process, some surfaces can become very thin locally. Application of decimation followed by refinement removes very small or thin triangles and segments the modified surfaces into parts which are then smoothed separately. The technique presented here for 3-D multi-scale surface smoothing is independent of the underlying triangulation. It is also argued that the proposed technique is preferable to *volumetric smoothing* or *level set methods*, since it is applicable to incomplete surface data which occurs during occlusion. Also, surfaces that are not simply connected or have holes do not pose any problem. Furthermore, due to employing 2-D convolutions rather than 3-D, this method is more efficient than other techniques.

INTRODUCTION

In this paper, a new technique is introduced for multi-scale shape description of free-form 3-D surfaces represented by polygonal or triangular meshes. Multi-scale descriptions have become very common in computer vision since they offer additional robustness with respect to noise and object detail along with more efficient processing. The multi-scale technique proposed here can be considered as a generalization of earlier multi-scale representation theories proposed for 2-D contours [1,2] and space curves [3]. However, the theoretical issues are significantly more challenging when working on free-form 3-D surfaces. Complete 3-D models of test objects have been used here, which can be constructed through automatic fusion of range images of the object obtained from different viewpoints [4].

When the technique of multi-scale smoothing of a 3-D object is used, its surface can be represented regardless of noise and shape distortions. The technique of multi-scale representation and recognition of 3-D surfaces is developed for viewpoint invariant identification and matching of 3-D objects. Geometric invariants are used to ensure that the shape representation for a 3-D object remains the same even after applying a rotation or uniform scaling [2,5]. The applications of this technique could be regarded as a navigational system for neurosurgical assistance, robot vision, provision of artificial eyes for the blind, microsurgery, aircraft navigation and virtual reality. Also, the prototyping and copying of complicated mechanical parts can be achieved through a 3-D range scanner.

In the approach considered here, diffusion of the surface is achieved through convolutions of local parameterizations of the surface with a 2-D Gaussian filter [6-8]. *Semigeodesic coordinates* [9] are utilized as a natural and efficient way of locally parameterizing

*. *Corresponding Author, Centre for Vision, Speech and Signal Processing, School of Electronic Engineering, Information Technology and Mathematics, University of Surrey, Guildford, GU2 7XH, UK.*

1. *Centre for Vision, Speech and Signal Processing, School of Electronic Engineering, Information Technology and Mathematics, University of Surrey, Guildford, GU2 7XH, UK.*

surface shape. The most important advantage of this method is that unlike other diffusion techniques such as volumetric diffusion [10,11] or level set methods [12], it has *local support* and is, therefore, applicable to partial data corresponding to surface-segments. This property makes it suitable for object recognition applications in the presence of occlusions. Another advantage of this method is its high efficiency, since 2-D rather than 3-D convolutions are employed in it.

The organization of this paper is as follows. First, a brief overview of previous work on 3-D object representations is provided. Then, the relevant theory from differential geometry and how a multi-scale shape description can be computed for a free-form 3-D surface are described. Both semigeodesic and geodesic polar coordinates are covered. Implementation issues encountered when adapting semigeodesic coordinates and geodesic polar coordinates to 3-D triangular meshes are also explained. Finally, diffusion results, discussion and the concluding remarks are presented.

LITERATURE SURVEY

In this section, a survey of previous work in representation of 3-D surfaces is presented. Sinha and Jain [13] provided an overview of geometry based representations derived from range data of objects. Representation schemes for 3-D objects have adopted some form of surface or volumetric parametric models to characterize the shape of the objects. Current volumetric representations rely on demonstrating objects in terms of general cylinders, superquadrics and set-theoric combinations of volume primitives as in Constructive Solid Geometry (CSG) or spatial occupancy [14-17]. However, it may not be possible to express objects with free-form surfaces using, for example, superquadric primitives. Although there are several methods available to model a surface, triangular meshes are the simplest and most effective form of polygons to cover a free-form surface. The common types of polygonal meshes include the triangular mesh [4,18] and the four sided spline patches.

Polyhedral approximations [19] fit a polyhedral object with vertices and relatively large flat faces to a 3-D object. A disadvantage is that the choice of vertices can be quite arbitrary which results in lack of robustness of the representation. Smooth 3-D splines [20] can also be fitted to 3-D objects. The shortcomings of this method are that the choice of knot points is again arbitrary and the spline parameters are not invariant. *Generalized cones* or *cylinders* [21] as well as *geons* [22] approximate a 3-D object using globally parameterized mathematical models, but they are not applicable to detailed free-form objects. In *volumetric diffusion* [10] or level set methods [12], an object is treated as a filled area or volume, which is then blurred by being subject to the diffusion equation. The boundary of each blurred object can then be defined by applying the Laplacian operator to the smoothed area or volume. The major shortcoming of these approaches is the lack of local support. In other words, the entire object data must be available. This problem makes them unsuitable for object recognition in the presence of occlusion. Another form of 3-D surface smoothing has been carried out in [23,24]. This method has drawbacks, since it is based on weighted averaging using neighboring vertices and, therefore, is dependent on the underlying triangulation. The smoothing of 3-D surfaces is a result of the diffusion process [25]. For parameterization of a 3-D surface, other methods have also been studied, such as the asymptotic coordinates [26], isothermic coordinates [9,27] and global coordinates [28] used for closed simply connected objects.

Global representations such as the Extended Gaussian Image (EGI) [29-31] describe 3-D objects in terms of their surface normal distributions on the unit sphere with appropriate support functions. However, arbitrary curved objects have to be either approximated by planar patches or divided into regions based on Gaussian curvature. Another approach for specifying a 3-D object is view-centered representations. The graph approach [32] attempts to group a set of infinite 2-D views of a 3-D object into a set of meaningful clusters of appearances. Murase and Nayar [33] and Swets [34] also have exploited photometric information to describe and recognize objects. Part based representations capture structure in object descriptions [35,36], but there is a lack of agreement in deciding the general set of part primitives that need to be used in order to be sufficient and appropriate.

SEMIGEODESIC AND GEODESIC POLAR PARAMETERIZATIONS

A crucial property of 2-D contours and space curves (or 3-D contours) is that they can be parameterized globally using the arclength parameter. However, free-form 3-D surfaces are more complex. As a result, no global coordinate system exists on a free-form 3-D surface which could yield a natural parameterization of that surface. Indeed, studies of local properties of 3-D surfaces are carried out in differential geometry using local coordinate systems called *curvilinear coordinates* or *Gaussian coordinates* [9]. Each system of curvilinear coordinates is introduced on a patch of a regular surface referred to as a *simple sheet.* A simple sheet of a surface is obtained from a rectangle by stretching, squeezing, and bending without tearing or glueing together. Given a parametric representation $\mathbf{r} = \mathbf{r}(u,v)$ on a local patch, the values of the parameters u and v determine the position of each point on that patch.

Geodesic Lines

Before the semigeodesic and geodesic polar coordinates can be described, it is necessary to define geodesic lines on a regular 3-D surface. The following definitions are useful [9,37]:

Definition 1

A geodesic line or a geodesic of a surface is a curve whose geodesic curvature is zero at every point. Geodesic curvature is the magnitude of the *vector of geodesic curvature.*

Definition 2

The vector of geodesic curvature of curve C lying on surface $\mathcal{S}$ at point P on C is obtained by projecting the *curvature vector* of C at P on the tangent plane to $\mathcal{S}$ at P.

Definition 3

The curvature vector of a curve C at point P is of the same direction as the principal normal vector at P and of length equal to the curvature of the curve at P.

Definition 4

The principal normal vector of curve C at point P is perpendicular to C at P and lies in the *osculating plane* at P. The plane with the highest possible order of contact with the curve C at point P is called the osculating plane at P.

The following crucial property of geodesic lines is actually utilized to construct geodesics on 3-D triangular meshes.

Minimal Property of Geodesics

An arc of geodesic line C passing through point P and lying entirely in a sufficiently small neighborhood of point P of surface $\mathcal{S}$ of class C_2 is the shortest join of P with any other point of C by a curve lying in the neighborhood.

Semigeodesic Coordinates

Semigeodesic coordinates at point P on surface $\mathcal{S}$ of class C_2 can be constructed in the following way:

- Choose a geodesic line C through point P in an arbitrary direction,
- Denote the arclength parameter on C by v, such that P corresponds to the value $v = 0$,
- Take further through every point of C, the geodesic line L perpendicular to C at the corresponding point,
- Denote the arclength parameter on L by u.

The two parameters, u and v, determine the position of each point in the domain swept out by these geodesic lines. It can be shown that in a sufficiently small neighborhood of point P, semigeodesic coordinates can always serve as curvilinear coordinates in a regular parametric representation of $\mathcal{S}$ [9]. The orthogonal cartesian coordinates in the plane are a special case of semigeodesic coordinates on a flat surface.

Geodesic Polar Coordinates

Geodesic polar coordinates can be constructed at point P on surface $\mathcal{S}$ of class C_2 in the following way:

- Choose an arbitrary direction $\mathbf{w}$ on $\mathcal{S}$ at point P,
- Consider all geodesic lines emanating from point P,
- Denote the arclength parameter on each geodesic in the previous step by v,
- Denote the angle between $\mathbf{w}$ and the tangent vector of each geodesic in Step 2 at point P by u,

Again, the two parameters, u and v, determine the position of each point in the domain swept out by these geodesic lines. It can be shown that in a sufficiently small neighborhood of point P (with P itself deleted), geodesic polar coordinates can always serve as curvilinear coordinates. Point P is a singular point of this parameterization since its coordinates are not uniquely defined. The polar coordinates in the plane are a special case of geodesic polar coordinates on a flat surface.

Gaussian Smoothing of a 3-D Surface

The procedures outlined above can be followed to construct semigeodesic coordinates or geodesic polar coordinates at every point of a 3-D surface. In the case of semigeodesic coordinates, local parameterization at each point P yields:

$$\mathbf{r}(u,v) = (x(u,v),\ y(u,v),\ z(u,v)).$$

The new location of point P is given by:

$$\mathbf{R}(u,v,\sigma) = (\mathcal{X}(u,v,\sigma),\ \mathcal{Y}(u,v,\sigma),\ \mathcal{Z}(u,v,\sigma)), \tag{1}$$

where:

$$\mathcal{X}(u,v,\sigma) = x(u,v) \otimes G(u,v,\sigma),$$

$$\mathcal{Y}(u,v,\sigma) = y(u,v) \otimes G(u,v,\sigma),$$

$$\mathcal{Z}(u,v,\sigma) = z(u,v) \otimes G(u,v,\sigma),$$

$$G(u,v,\sigma) = \frac{1}{2\pi\sigma^2} e^{-\frac{(u^2+v^2)}{2\sigma^2}}, \tag{2}$$

and $\otimes$ denotes convolution. In the case of geodesic polar coordinates, the Gaussian function becomes one-dimensional. As a result, each of the 2-D convolutions

above can be expressed as a series of 1-D convolutions. In either case, this process is repeated at each point of $\mathcal{S}$. After filtering, the new point positions define the coordinates of the smoothed surface. Since the constructed coordinates are valid locally, the Gaussian filters always have $\sigma = 1$.

Multi-Scale Description of a 3-D Surface via Diffusion

In order to achieve multi-scale descriptions of a 3-D surface, the surface has to be smoothed according to the process described earlier. The smoothed surface is then considered as the input to the next stage of smoothing. This procedure is then iterated many times to obtain multi-scale descriptions of $\mathcal{S}$. This process is equivalent to diffusion smoothing:

$$\frac{\partial \mathcal{S}}{\partial t} = H\,\mathbf{n}, \tag{3}$$

since the Gaussian function satisfies the heat equation. In the above equation, t is time, H is mean curvature and $\mathbf{n}$ is the surface normal vector. t can be regarded as the number of iterations.

IMPLEMENTATION ON A 3-D TRIANGULAR MESH

The theory explained in the previous section must be adapted to a 3-D triangular mesh. Both semigeodesic and geodesic polar coordinates involve construction of geodesic lines. Clearly the segment of a geodesic that lies on any given triangle is a straight line. Two situations must be considered that are being addressed in Theorems 1 and 2:

- Extension of a geodesic when it intersects a triangle edge,
- Extension of a geodesic when it intersects a triangle vertex.

Theorem 1

Suppose a geodesic intersects an edge e shared by triangles T_1 and T_2. The extension of this geodesic beyond e is obtained by rotating T_2 about e so that it becomes co-planar with T_1, extending the geodesic in a straight line on T_2, and rotating T_2 about e back to its original position.

Proof

Assume by contradiction that the procedure above does not construct a geodesic. Let g_1 be the segment of the geodesic on T_1 and let g_2 be the segment of the geodesic on T_2. Rotate T_2 about e so that it becomes co-planar with T_1. According to the assumption, g_1 and g_2 will not be co-linear. Hence, for point P_1 on g_1 and point P_2 on g_2, there will be a shorter path from P_1 to P_2. This is the straight line joining P_1 to P_2. Now rotate T_2 back to its original position. The length of the path just constructed remains the same, so it will still be shorter than the geodesic from P_1 to P_2. A contradiction has been reached. Therefore, the procedure described correctly constructs a geodesic. Note that the construction above extends to several triangles as long as they remain in a local neighborhood.

Theorem 2

Suppose a geodesic arrives at vertex V of the mesh. Define the normal vector $\mathbf{n}$ at V as the average of the surface normals of all the triangles incident on V weighted by the incident angle. Let Q be the plane formed by the geodesic incident on V and $\mathbf{n}$. The extension of this geodesic beyond V is found by intersecting Q with the mesh.

Proof

The curvature vector k of the path obtained by the above procedure lies in Q. k is also perpendicular to tangent plane T (which is defined as perpendicular to $\mathbf{n}$ at V). The vector of geodesic curvature of the path is obtained by projecting k onto the tangent plane. It follows that geodesic curvature of the path is zero. Hence, the path is a geodesic line.

Construction of Geodesic Line on a Triangular Mesh

Since triangular meshes are used to model 3-D surfaces, the construction of a geodesic line on a triangular mesh is first explained. Figure 1 shows the triangles CDE and GDC with common edge CD on a triangular mesh. If a geodesic line is required between two arbitrary points A and B, the triangle GDC is rotated at the common edge CD until both triangles CDE and GDC are co-planar. The straight line AB' is the shortest line joining points A and B'.

On the triangles CDE and $G'DC$, the geodesic line AB' intersects the common edge CD. At the intersection I, the opposite angles ψ and ϕ are equal. The angle ϕ is the direction of segment IB' of geodesic line on the triangle $G'DC$. When rotating the triangle $G'DC$ back to the position of triangle GDC, the length of AB does not increase and it is still the shortest line. The angle ϕ at the common edge CD determines the direction of the segment IB of the geodesic line and the angle ψ_1 of the segment IB at the new common edge DG provides the new intersection angle. Thus,

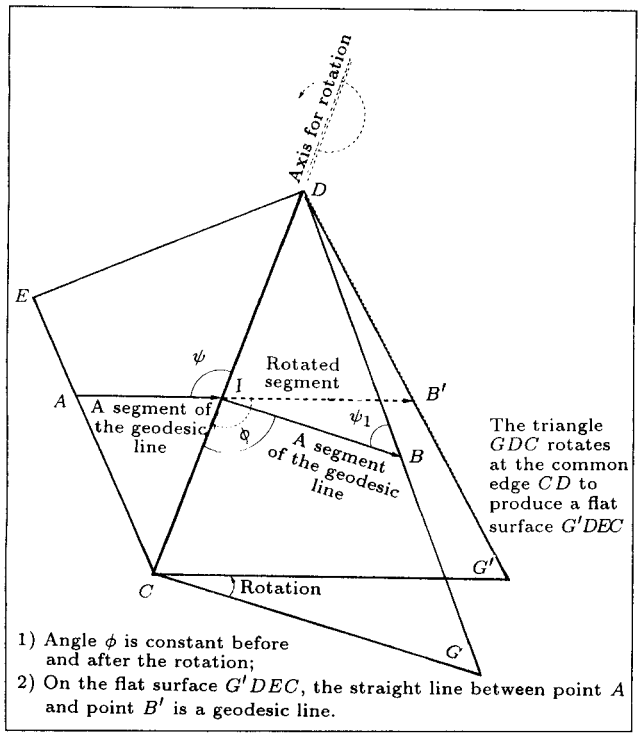

Figure 1. Geodesic line on a triangular mesh.

the next segment of the geodesic line can be created. Therefore, a complete geodesic line on this local patch is generated.

Arbitrary Direction of a Geodesic Line

Before semigeodesic coordinates can be generated on a local patch at a chosen vertex B, an arbitrary geodesic line is required. Since the direction of the arbitrary geodesic line can be randomly selected, the edge between vertex B and the first neighbor F is chosen as the arbitrary direction, shown in Figure 2.

The next step is to create an arbitrary geodesic line from the vertex B. The construction of the positive portion $+u$ of the arbitrary geodesic line can now begin. First, weighted average normal vector W at vertex B is generated from the unit normal n_i and the vertex angle α_i of neighboring triangles.

$$W = \frac{\sum_{i=1}^{m} \alpha_i n_i}{\sum_{i=1}^{m} \alpha_i}, \tag{4}$$

where m is the number of neighboring triangles. Therefore, a normal plane $N(B)$ is defined by the weighted average normal unit vector W and the arbitrary direction FB. The intersection I between this normal plane $N(B)$ and the opposite edge CD produces the first segment BI of the arbitrary geodesic line. Then, each segment used in the construction of the geodesic line is sampled at equally spaced intervals. The number of sample points depends on the sample step size and the length of the current segment. The sampling interval is normally equal to the average edge length L of the triangular mesh. Furthermore, a perpendicular direction P_iS_i and the closest vertex at each sample point S_i are generated and stored for the construction of second family of lines, where i is the sample point number. For a filter size of 9, i ranges from -4 to $+4$. The negative portion $-u$ of the arbitrary geodesic line can be constructed from the same vertex B by applying the same construction procedure for the positive portion $+u$. Then, these two portions are joined together to form a completed arbitrary geodesic line on the mesh.

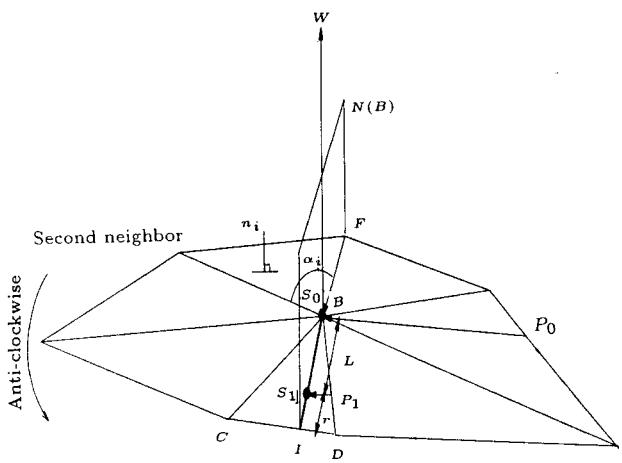

Figure 2. The first segment of the arbitrary geodesic line.

Adjustment of an Arbitrary Geodesic Line

It is possible that an arbitrary geodesic line could lie near and almost parallel to an edge. It is also possible for a sample point to be very close to a vertex or edge. In these cases, the failure to find the intersection of the parallel lines or the failure to calculate the distance between very close points may result in a computational fault. Therefore, a fine adjustment to the direction of the arbitrary geodesic line or the position of a sample point is required. The criterion for this adjustment is based on the threshold of the average edge length L. Figure 3 shows that if the angle α between segment VI of the arbitrary geodesic line and edge VU is very small, the segment VI and the edge VU are almost parallel. Thus, the segment VI can be adjusted and placed over the edge VU. Similarly, if the sample point S_1 is very close to the edge MK and the sample point S_2 is very near to the vertex V, the sample point S_1 can be moved on the edge MK and the sample point S_2 can be moved to the vertex V.

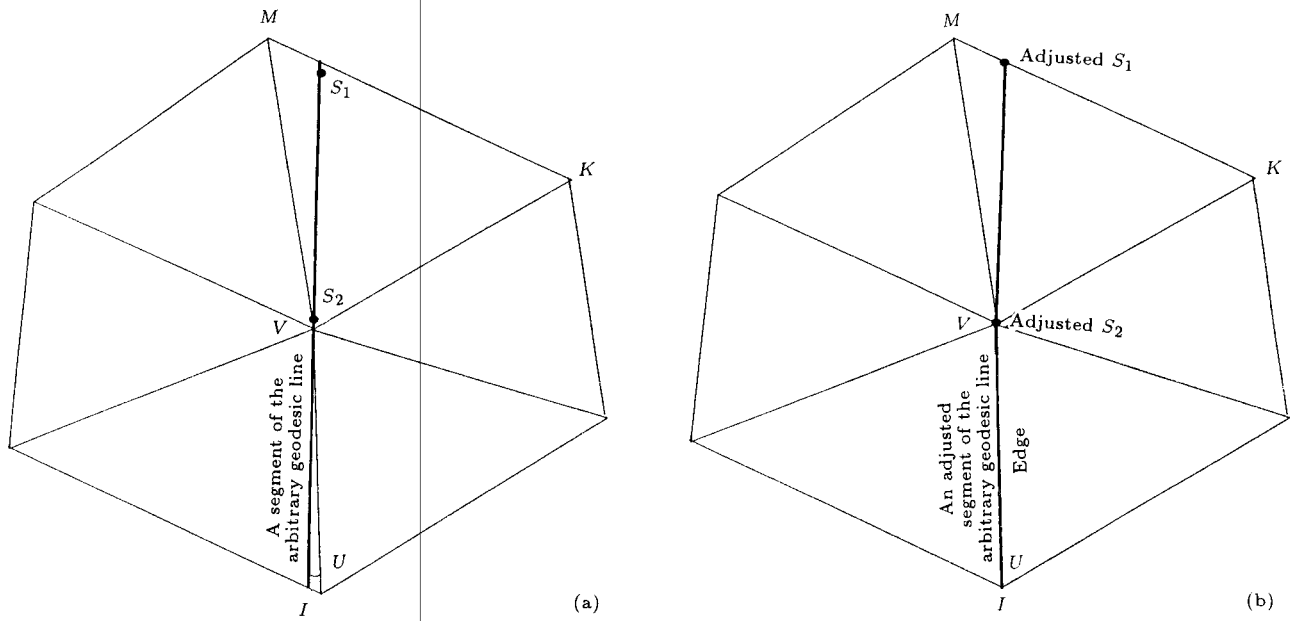

Figure 3. The adjustment of the arbitrary geodesic line and the sample points.

Construction of Perpendicular Direction

For the construction of the perpendicular direction, many different conditions have to be considered. If a sample point is placed on vertex S, normal plane $N(S)$ can be created by the weighted average normal vector W at the vertex, given by Equation 4, and segment SI of the arbitrary geodesic line, as shown in Figure 4.

The perpendicular direction PS on the surface is obtained by rotating the normal plane 90 degrees anti-clockwise from the segment SI of the arbitrary geodesic line. This rotated normal plane is then intersected with the edge of a neighboring triangle.

When a sample point resides on an edge of a triangle, three different cases arise for constructing the perpendicular directions: 1) If the segment IS of the arbitrary geodesic line and the edge CD are orthogonal, then a segment of the edge CD becomes the perpendicular direction PS (see Figure 5a); 2) If the angle ϕ between the segment IS of the arbitrary geodesic line and the edge CD is less than 90 degrees as shown in Figure 5b, then the perpendicular direction PS is produced by rotating the segment IS by 90 degrees anti-clockwise (in this case, the rotated segment intersects with an edge on the same triangle CDE); 3) If the angle ϕ is greater than 90 degrees, then the segment IS is rotated 90 degrees clockwise. In this case, the rotated segment intersects with an edge on the same triangle CDE to produce a segment $P'S$ of the pseudo geodesic line (see Figure 5c). The segment $P'S$ is extended from the triangle CDE to the triangle GDC by using the construction techniques of an arbitrary geodesic line mentioned earlier. The extended segment PS becomes the perpendicular direction of the arbitrary geodesic line. This simplifies the procedure of constructing a perpendicular direction on a triangular mesh.

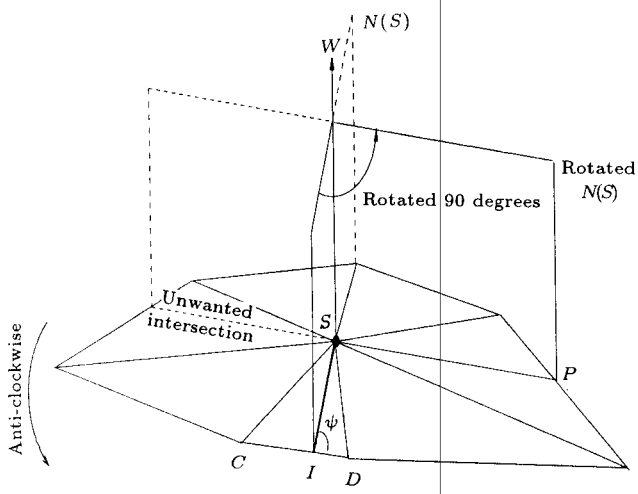

Figure 4. A perpendicular direction of an arbitrary geodesic line.

When the segment II' of the arbitrary geodesic line lies on the common edge CD, the perpendicular direction PS at the sample point S is defined by rotating the common edge CD on the right hand side triangle GDC, 90 degrees anti-clockwise at the sample point S (see Figure 6a). Finally, if a sample point S is inside a triangle, the perpendicular direction PS is defined by simply rotating the segment II' of the arbitrary geodesic line 90 degrees anti-clockwise at the sample point S as shown in Figure 6b.

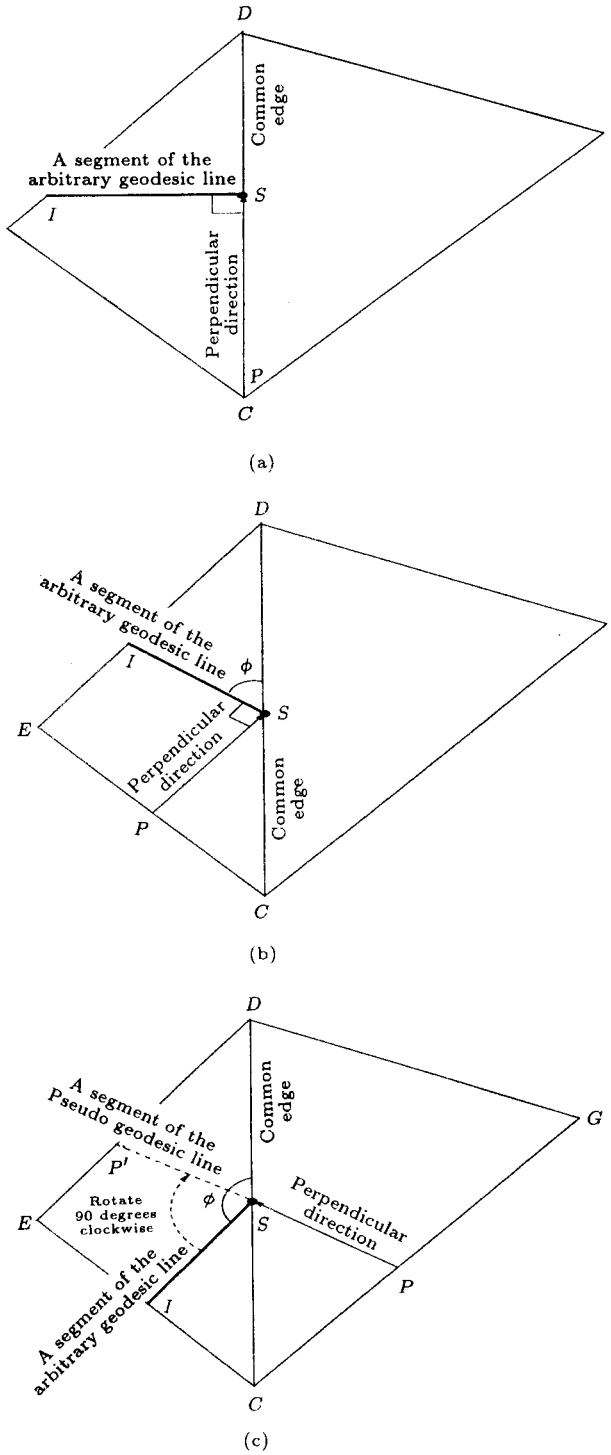

Figure 5. Creation of a perpendicular direction of the arbitrary geodesic line when a sample point resides on an edge of a triangle.

Implementation of Semigeodesic Coordinates

Semigeodesic coordinates can now be constructed at each vertex of the mesh which becomes the local origin. The following procedure is employed:

- Construct a geodesic from the origin in the direction of one of the incident edges,
- Construct the other half of that geodesic by extending it through the origin in the reverse direction using the procedure outlined in Theorem 2,
- Parameterize the geodesic by the arclength parameter at regular intervals to obtain a sequence of sample points. The sampling interval should be proportional to the average edge length,
- At each sample point on the first geodesic, construct a perpendicular geodesic and extend it in both directions,
- Parameterize each of the geodesics constructed in the previous step by the arclength parameter at regular intervals. The sampling interval should be equal to what was used in Step 3.

Figure 7 shows the complete semigeodesic coordinates on a triangular mesh.

Due to the displacement of vertices which occurs as a result of smoothing, very small and/or very thin triangles can be generated during smoothing. These odd triangles can cause computational problems and are, therefore, removed or merged with neighboring triangles using known existing algorithms for mesh decimation and refinement [38]. Detection of these triangles is based on the length of the shortest side or the smallest angle. When the smallest side or the smallest angle of a triangle is less than a small threshold, that triangle is removed by merging it with neighboring triangles. Decimation and refinement are applied after each iteration to simplify the mesh. As a result, the number of triangles gradually decreases during smoothing. It is also possible for a surface to become very thin locally as a result of smoothing. When this happens, smoothing cannot continue without segmentation of the surface into parts. Such a segmentation also occurs as a result of mesh decimation and refinement, since the thinned area of the surface always consists of very small and thin triangles. Smoothing can then continue after segmentation with each part of the object smoothed independently.

Implementation of Geodesic Polar Coordinates

Geodesic polar coordinates are also constructed at each vertex of the mesh which again becomes the local origin. The following procedure is used:

- Construct a geodesic from the origin in an arbitrary direction such as the direction of one of the incident edges,
- Let N be the normal plane at the origin defined by the geodesic constructed in the previous step and the normal vector $\mathbf{n}$ defined in Theorem 2,
- Rotate N about $\mathbf{n}$ by angle α and intersect it with the mesh to obtain the next geodesic emanating from the origin,

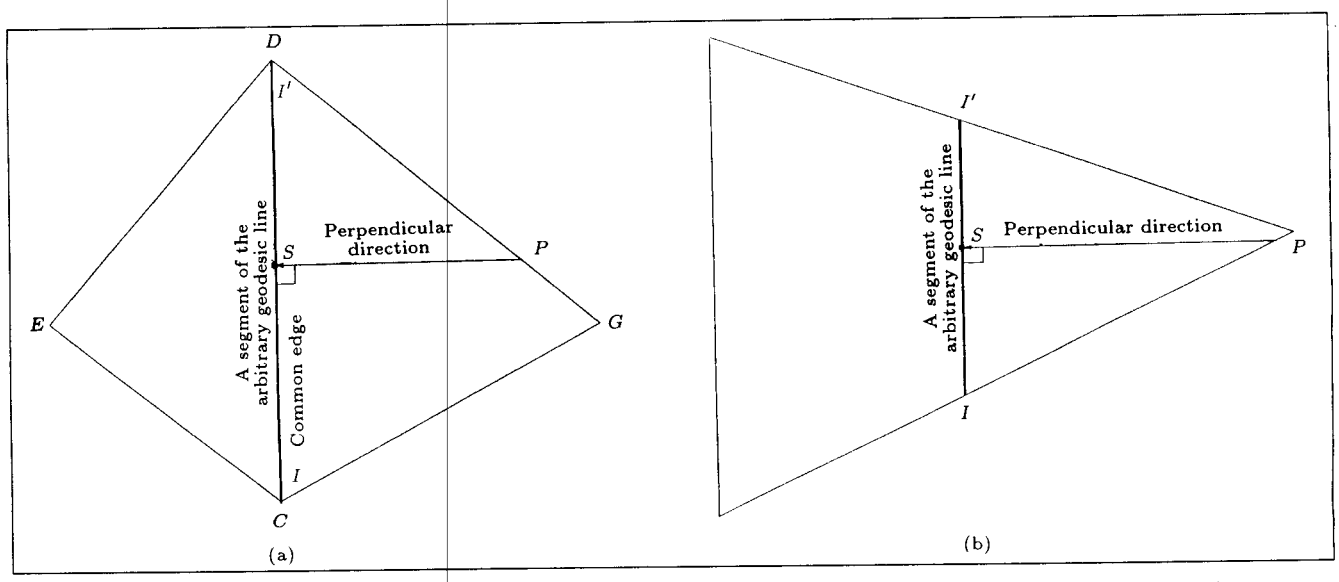

Figure 6. Creation of a perpendicular direction from the segment of the arbitrary geodesic line which lies on the common edge of the triangles.

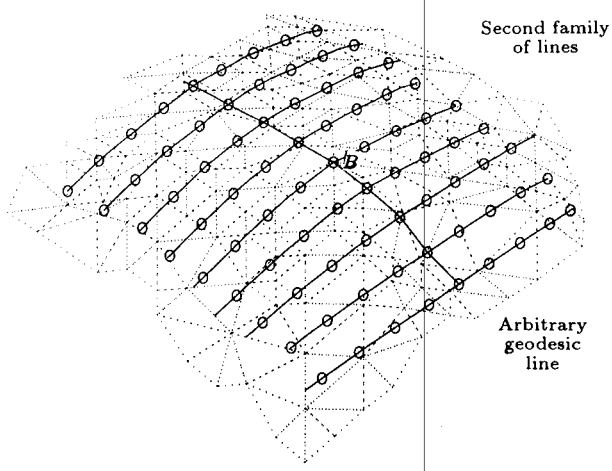

Figure 7. A completed semigeodesic coordinates on a triangular mesh.

- Repeat the previous step until N is back in its original position,
- Parameterize each of the constructed geodesics by the arclength parameter at regular intervals to obtain a sequence of sample points on each geodesic. The sampling interval should be proportional to the average edge length.

Semigeodesic Coordinates on Open Surfaces

Quite often, due to occlusion or complex object shape, it is not possible to construct complete and closed surfaces. As a result, the algorithm described above should be modified to make it also applicable to open surfaces. The algorithm for smoothing an open surface is defined in the following way:

- Grid construction and smoothing at internal vertices is carried out as on closed surfaces. Any geodesic line that reaches the boundary will stop. The last sample point at or near the boundary will be duplicated until the grid is filled. Likewise, if some geodesic lines cannot be constructed, the last geodesic line near the boundary will be duplicated until the grid is filled;
- If the vertex V of triangle T resides on the boundary, measure the angle α between the two edges of T that are incident on V. Choose the first geodesic line as the bisector of α. Only half of the first geodesic line is constructed because the other half falls outside the surface boundary;
- At the same vertex, construct another geodesic line perpendicular to the first one;
- One of those geodesic lines might soon intersect the boundary, so compare the lengths of those lines and choose the longer one. This allows the maximum size grid to be constructed;
- Construct the second family of geodesic lines as perpendicular to the longer geodesic line determined above;
- As before, any geodesic line that reaches the boundary will stop, and the last sample point at or near the boundary will be duplicated until the grid is filled.

RESULTS AND DISCUSSION

The smoothing routines were implemented entirely in C++. Complete triangulated models of 3-D objects used for the presented experiments were con-

structed [4]. In order to experiment with these techniques, both simple and complex 3-D objects with a different number of triangles were used. Each iteration of smoothing of a surface with 1000 vertices takes about 0.5 second of CPU time on an UltraSparc 170E.

The first test object was a cube with 98 vertices and 192 triangles. The smoothing results using semigeodesic coordinates (with filter size equal to 9) are shown in Figures 8a and b. The original cube is changed to a sphere after five iterations. The experiment was also repeated using geodesic polar coordinates (with 9 polar lines) and the smoothing results are shown in Figures 8c and d. These results indicate that smoothing using semigeodesic coordinates and geodesic polar coordinates produce similar outcomes. Therefore, this smoothing technique, using semigeodesic coordinates with filter size equal to 9, is applied to the following 3-D surfaces.

The second test object was a foot with 2898 triangles and 1451 vertices. The smoothing results are shown in Figure 9. The foot becomes rounded iteratively and evolves into an ellipsoidal shape after 100 iterations. Now the technique is examined with more complex 3-D objects.

Figure 10 shows the third test object which was a telephone handset with 11124 triangles and 5564 vertices. Notice that the surface noise is eliminated iteratively with the object becoming smoother gradually and after 15 iterations the object becomes very thin in the middle. Decimation and refinement then removes the thin handset and segments the object into two parts. Smoothing then continues for each part as shown in Figure 11.

The fourth test object was a chair with 3788

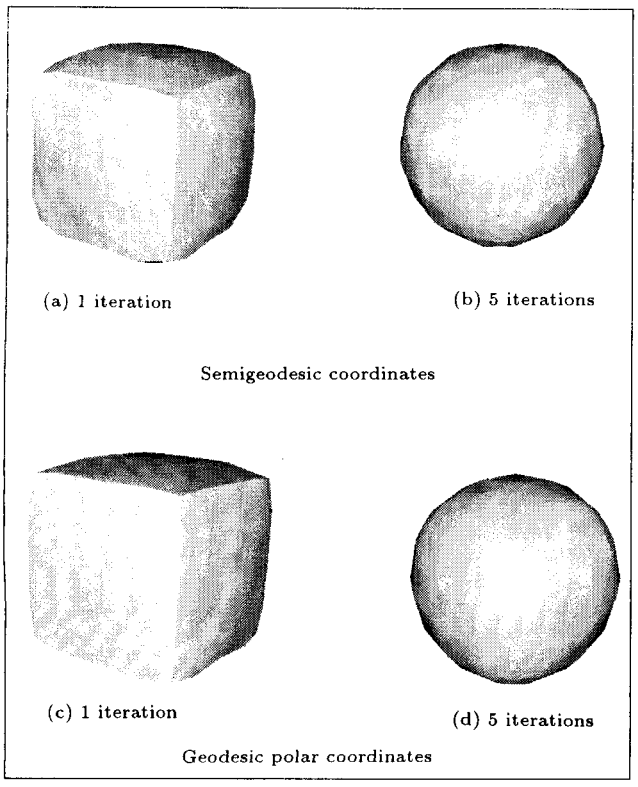

Figure 8. Smoothing of the cube.

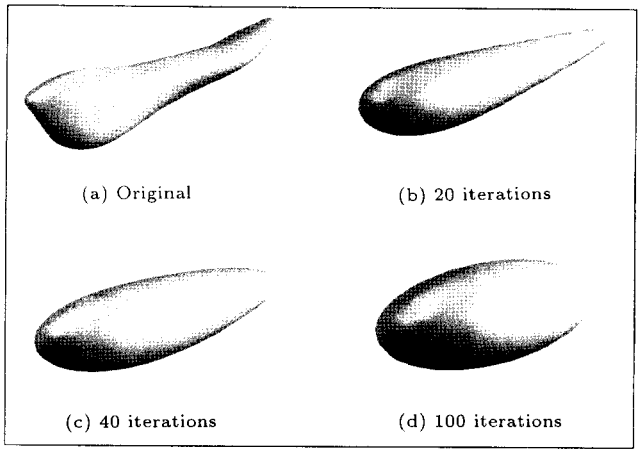

Figure 9. Diffusion of the foot.

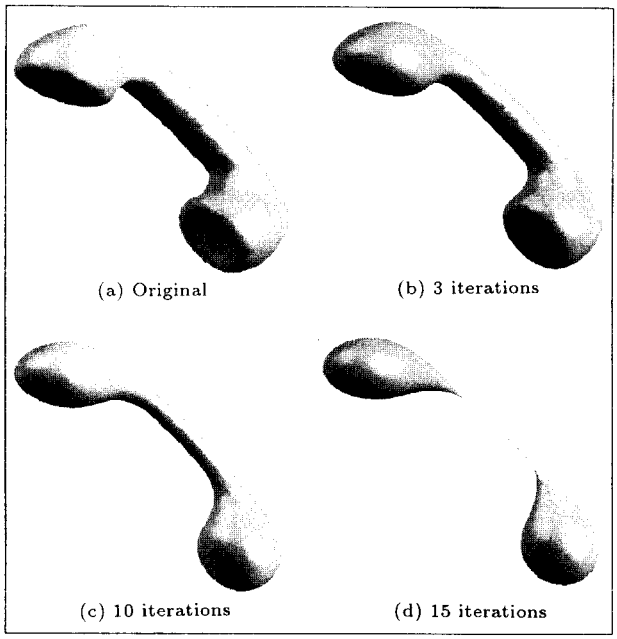

Figure 10. Diffusion of the telephone handset.

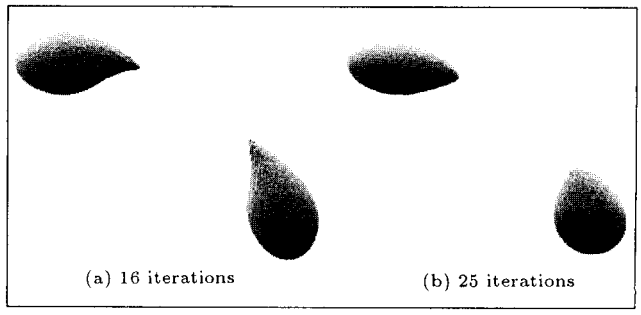

Figure 11. Smoothing of the segmented phone handset.

triangles and 1894 vertices as shown in Figure 12, where again the legs of the chair become thin after 4 iterations as observed for the phone handset. The thin legs are then removed and the object is segmented into two parts, where after smoothing each part the results are shown in Figure 13.

The method is then applied to more complex objects. The next test object was a cow with 3348 triangles and 1676 vertices as shown in Figure 14. The surface noise is eliminated iteratively with the object becoming smoother gradually, where after 8 iterations the legs, ears and tail are removed.

The last test object was a dinosaur with 2996 triangles and 1500 vertices as shown in Figure 15. The object becomes smoother gradually and the legs, tail and ears are removed after 20 iterations, as seen for the cow.

These examples demonstrate that the technique

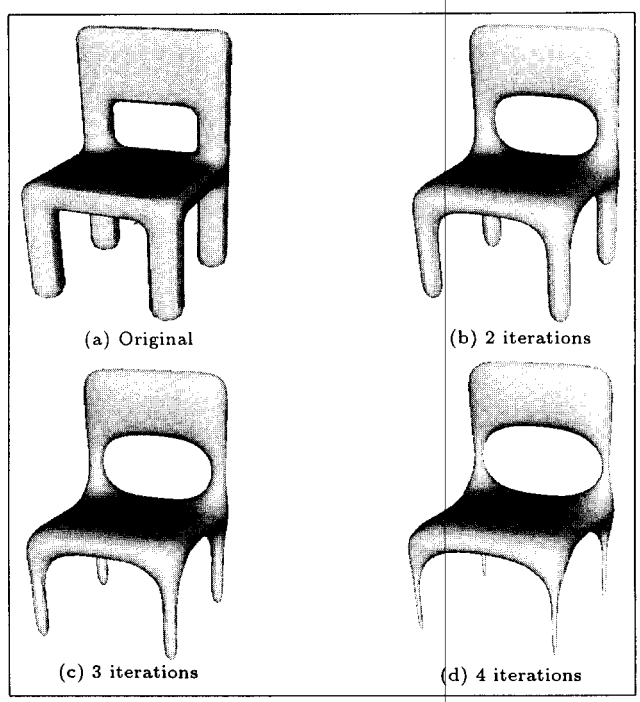

Figure 12. Smoothing of the chair.

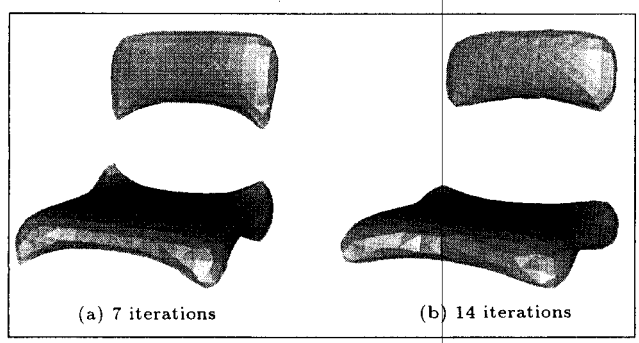

Figure 13. Smoothing of the segmented chair.

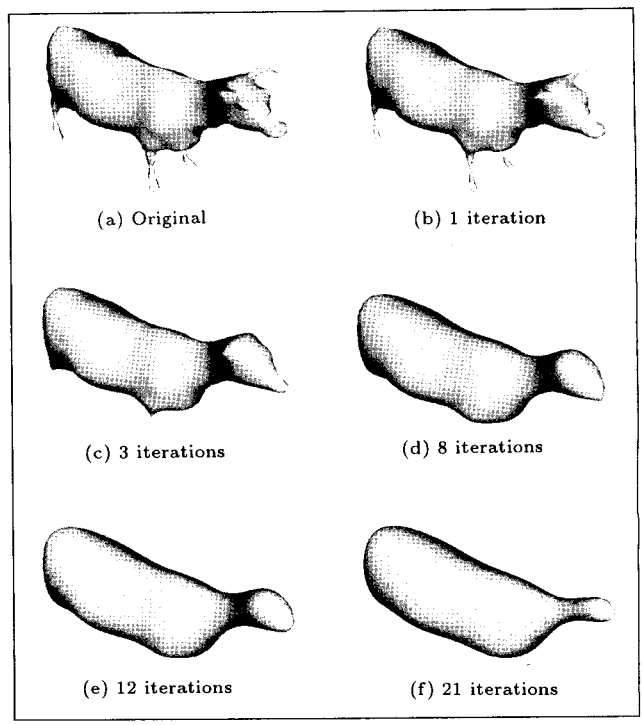

Figure 14. Smoothing of the cow.

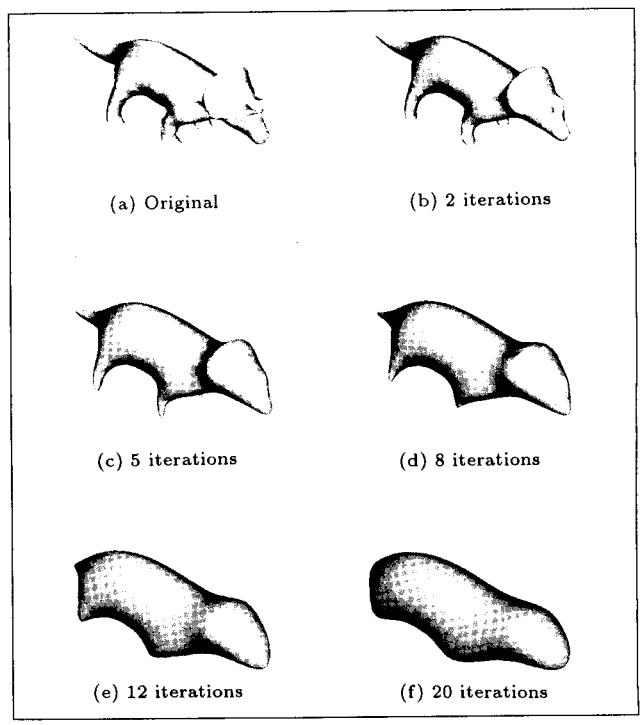

Figure 15. Smoothing of the dinosaur.

presented here is effective in eliminating surface noise as well as removing surface detail. The result is a gradual simplification of object shape. Animation of surface diffusion can be observed at the following web site: http://www.ee.surrey.ac.uk/Research/VSSP/ demos/css3d/index.html.

This smoothing technique was also applied to a

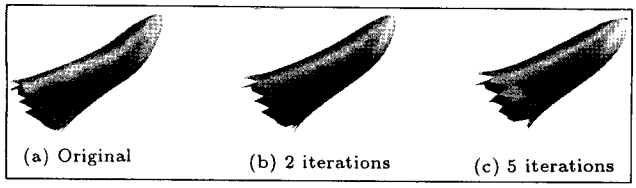

Figure 16. Diffusion of the partial foot.

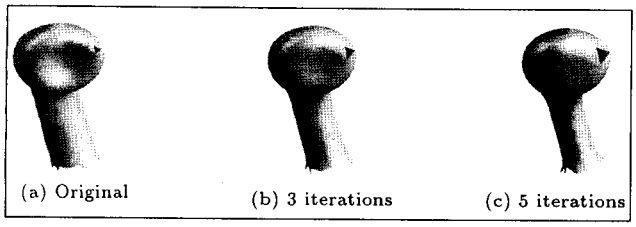

Figure 17. Diffusion of the partial telephone handset.

number of open/incomplete surfaces. Figure 16 shows the smoothing results obtained for a part of the foot object in Figure 9. Figure 17 illustrates the results for a part of the telephone handset in Figure 11. This object also has a triangle removed in order to generate an internal hole. Figure 18 depicts the smoothing results found for the lower part of the chair object in Figure 12. Figure 19 shows smoothing results obtained for a partial rabbit. The object is smoothed iteratively and the ears disappear as well.

CONCLUDING REMARKS

In this paper, a novel technique for multi-scale smoothing of a free-form triangulated 3-D surface was presented. The method was independent of the underlying triangulation. This was achieved by convolving local parameterizations of the surface with 2-D Gaussian filters iteratively. The method for local parameterization made use of semigeodesic and geodesic polar coordinates as natural and efficient ways of sampling the local surface shape. It was shown that smoothing techniques using semigeodesic coordinates and geodesic polar coordinates produce similar results. The smoothing eliminated the surface noise and small surface details gradually and resulted in simplification of the object shape. During smoothing some surfaces can become very thin locally. Application of decimation followed by refinement removes very small/thin triangles and segments those surfaces into parts which are then smoothed separately. The approach is preferable for volumetric smoothing or level set methods since it is applicable to incomplete surface data which occurs during occlusion. Finally, surfaces with holes and surfaces that are not simply connected do not pose any problems.

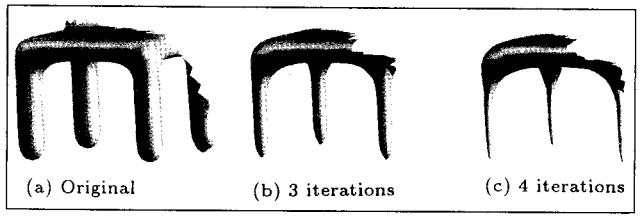

Figure 18. Smoothing of the partial Chair.

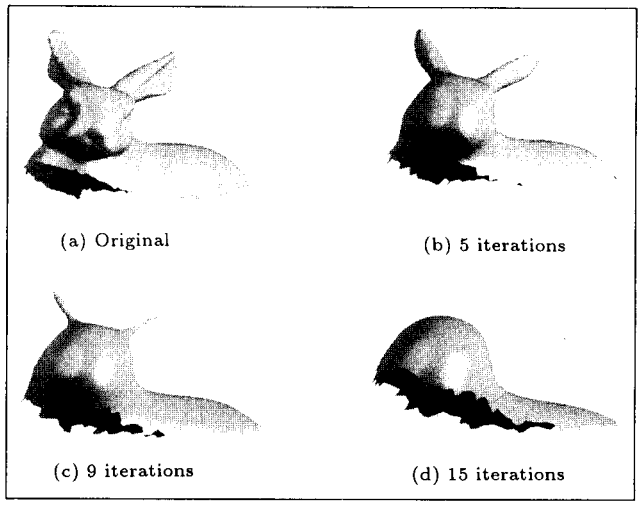

Figure 19. Smoothing of the rabbit head.

REFERENCES

1. Mokhtarian, F. and Mackworth, A.K. "Scale-based description and recognition of planar curves and two-dimensional shapes", *IEEE Trans Pattern Analysis and Machine Intelligence*, **8**(1), pp 34-43 (1986).
2. Mokhtarian, F. and Mackworth, A.K. "A theory of multi-scale, curvature-based shape representation for planar curves", *IEEE Trans Pattern Analysis and Machine Intelligence*, **14**(8), pp 789-805 (1992).
3. Mokhtarian, F. "A theory of multi-scale, torsion-based shape representation for space curves", *Computer Vision and Image Understanding*, **68**(1), pp 1-17 (1997).
4. Hilton, A., Stoddart, A.J., Illingworth, J. and Windeatt, T. "Reliable surface reconstruction from multiple range images", in *Proc. European Conference on Computer Vision*, Cambridge, UK, pp 117-126 (1996).
5. Sonka, M., Hlavac, V. and Boyle, R., *Image Processing, Analysis, and Machine Vision*, Chapman and Hall, London, UK (1993).
6. Mokhtarian, F., Khalili, N. and Yuen, P. "Multi-scale 3-d free-form surface smoothing", in *Proc. British Machine Vision Conference*, pp 730-739 (1998).
7. Mokhtarian, F., Khalili, N. and Yuen, P. "Multi-scale free-form surface description", in *Proc. Indian Conference on Computer Vision, Graphics and Image Processing*, pp 70-75, New Delhi, India (1998).
8. Yuen, P., Mokhtarian, F. and Khalili, N. "Multi-scale 3-d surface description: open and closed surfaces", in

Scandinavian Conference on Image Analysis, pp 303-310, Green-land (1999).

9. Goetz, A., *Introduction to Differential Geometry*, Addison-Wesley, Reading, MA, USA (1970).
10. Koenderink, J.J., *Solid Shape*, MIT Press, Cambridge, MA, USA (1990).
11. Koenderink, J.J. and Vandoorn, A.J. "Dynamic shape", *Biological Cybernetics*, **53**, pp 383-396 (1986).
12. Sethian, J.A., *Level Set Methods*, Cambridge University Press (1996).
13. Sinha, S.S. and Jain, R. "Range image analysis", in *Handbook of Pattern Recognition and Image Processing: Computer Vision*, T.Y. Young, Ed., **2**, pp 185-237 (1994).
14. Pentland, A.P. "Perceptual organisation and the representation of natural form", *Artificial Intelligence*, **28**, pp 293-331 (1986).
15. Solina, F. and Bajcsy, R.K. "Recovery of parametric models from range images: The case for superquadries with global deformations", *IEEE Trans. on Pattern Analysis and Machine Intelligence*, **12**, pp 131-147 (1990).
16. Chen, T.W. and Lin, W.C. "A neural network approach to csg-based 3-d object recognition", *IEEE Trans. on Pattern Analysis and Machine Intelligence*, **16**(7), pp 719-726 (1994).
17. Samet, H., *The Design and Analysis of Spatial Data Structures*, Addison-Wesley (1990).
18. Hilton, A., Stoddart, A.J., Illingworth, J. and Wincleatt, T. "Marching triangles: Range image fusion for complex object modelling", in *Proc. IEEE International Conference on Image Processing*, Lausanne, Switzerland, pp 381-384 (1996).
19. Faugeras, O.D. and Hebert, M. "The representation, recognition, and locating of 3-d objects", *Int. J. of Robotics Research*, **5**(3), pp 27-52 (1986).
20. Stoddart, A.J. and Baker, M. "Reconstruction of smooth surfaces with arbitrary topology adaptive splines", in *Proc. ECCY* (1998).
21. Soroka, B.I. and Bajcsy, R.K. "Generalized cylinders from serial sections", in *Proc. International Joint Conference on Pattern Recognition* (1976).
22. Pilu, M. and Fisher, R. "Recognition of geons by parametric deformable contour models", in *Proc. European Conference on Computer Vision*, pp 71-82, Cambridge, UK (1996).
23. Taubin, G. "Curve and surface smoothing without shrinkage", in *Proc. ICCY* (1995).
24. Taubin, G., Zhang, T. and Golub, G. "Optimal surface smoothing as filter design", in *Proc. ECCY*, pp 283-292 (1996).
25. ter Haar Romeny, B.M., *Geometry Driven Diffusion in Computer Vision*, Kluwer Academic (1994).
26. Kreyszig, E., *Differential Geometry*, Oxford University Press, UK (1959).
27. Chern, S.S., Hartman, P. and Wintner, A. "On isometric coordinates", in *Commentaries Mathematical Helvetici*, **28** (1954).
28. Brechbuhler, C., Gerig, G. and Kubler, O. "Parameterization of closed surfaces for 3-d shape description", *Computer Vision and Image Understanding*, **61**(2), pp 154-170 (1995).
29. Horn, B.K.P. "Extended gaussian images", *Proc. of the IEEB*, **72**(12) (1984).
30. Kang, S.B. and Ikeuchi, K. "The complex egi, a new representation for 3-d pose determination", *IEEE Trans Pattern Analysis and Machine Intelligence*, **15**(7), pp 707-721 (1993).
31. Liang, P. and Taubes, C.H. "Orientation-based differential geometric representations for computer vision applications", *IEEE Trans Pattern Analysis and Machine Intelligence*, **16**(3), pp 249-258 (1994).
32. Koenderink, J.J. and Vandoorn, A.J. "Internal representation of solid shape with respect to vision", *Biological Cybernetics*, **32**(4), pp 211-216 (1979).
33. Murase, H. and Nayar, S.K. "Visual learning and recognition of 3-d objects from appearance", *International Journal of Computer Vision*, **14**(1), pp 5-24 (1995).
34. Swets, D.L. "The self-organising hierarchical optimal subspace learning and inference framework for object recognition", in Ph.D. Thesis, Michigan State University, Dept of Computer Science, Michigan, USA (1996).
35. Raja, M.S. and Jain, A.K. "Obtaining generic parts from range images using a multi-view representation", *Computer Vision, Graphics and Image Processing*, **60**, pp 44-64 (1994).
36. Dickinson, S.J., Pentland, A.P. and Rosenfeld, A. "3-d shape recovery using distributed aspect matching", *IEEE Trans. on Pattern Analysis and Machine Intelligence*, **14**, pp 174-198 (1992).
37. Heitzz, S., *Coordinates in Geodesy*, Addison-Wesley, Berlin, Germany (1985).
38. Hoppe, H. "Progressive meshes", in *Proc. SIGGRAPH*, pp 99-106 (1996).